Triple para -Functionalized Cations and Neutral Radicals of Enantiopure Diaza[4]helicenes

Fabri, Bibiana; Funaioli, Tiziana; Frederic, Lucas Dan; Elsner, Christina Mareike; Bordignon, Enrica; Zinna, Francesco; Di Bari, Lorenzo; Pescitelli, Gennaro; Lacour, Jérôme

Triple *para*-Functionalized Cations and Neutral Radicals of Enantiopure Diaza [4]Helicenes

Bibiana Fabri,[a] Tiziana Funaioli,[b] Lucas Frédéric,[a#] Christina Elsner,[c] Enrica Bordignon,[c] Francesco Zinna,[b] Lorenzo Di Bari,[b] Gennaro Pescitelli,[b] Jérôme Lacour*[a]

[a] *Department of Organic Chemistry and* [c] *Department of Physical Chemistry, University of Geneva, Quai Ernest Ansermet 30, 1211 Geneva 4 (Switzerland)*

[b] *Dipartimento di Chimica e Chimica Industriale, University of Pisa, Via G. Moruzzi 13, 56124 Pisa (Italy)*

*Email: jerome.lacour@unige.ch

ABSTRACT: Modulation of absorbance and emission is key for the design of chiral chromophores. Accessing a series of compounds absorbing and emitting (circularly polarized) light over a wide spectral window, and often toward near infrared, is of practical value in (chir)optical applications. Herein, by late-stage functionalization on derivatives bridging triaryl methyl and helicene domains, we have achieved the regioselective triple introduction of *para* electron-donating or electron-withdrawing substituents. Extended tuning of electronic (*e.g.*, $E_{1/2}^{red}$ –1.50 V → –0.68 V) and optical (*e.g.*, emission covering from 550 to 850 nm) properties is achieved for the cations and neutral radicals; the latter compounds being easily prepared by mono electron reductions under electrochemical or chemical conditions. While luminescence quantum yields can be increased up to 70% in the cationic series, strong Cotton effects are obtained for certain radicals at low energies (λ_{abs} ~ 700-900 nm) with g_{abs} values above 10^{-3}. The open-shell electronic nature of the radicals was further characterized by EPR revealing an important spin density delocalization that contributes to their persistence.

INTRODUCTION

Organic dyes offer extensive molecular control over optical and electronic properties and hence represent attractive research targets. Of particular interest is the design and characterization of stable carbocations and organic open-shell radicals useful in many applications.[1,2] Importantly, when redox active, these compounds may exist in multiple oxidation states.[3] Recently, special interest has been focused on neutral organic radicals, which present a doublet spin configuration in both ground and excited states, with possible applications in optoelectronics.[4] Furthermore, if chiral, these cationic and/or radical structures possess additional magnetic and chiroptoelectronic properties such as electronic circular dichroism (ECD), circularly polarized luminescence (CPL) and possibly chiral induced spin selectivity (CISS) that can be useful for further developments.[5]

In this context, triaryl methyl derivatives constitute an important class of molecular structures able to stabilize cationic or radical species, and presenting structural features related to chirality (Figure 1, **A** and **B**).[6,7] In fact, in recent years, one of the most studied classes of stable organic radicals is that of polychlorinated trityls **I**.[8] Most of these unbridged trityl derivatives present asymmetric three-bladed propeller geometries.[9] However, resolution into single enantiomers is difficult due to low or moderate configurational stability of the adducts,[10] to a few exceptions such as the polybrominated trityl radical for which ECD and CPL measurements could be performed.[11] To offset the issue of configurational lability, chiral substituents can be attached to the skeletons.[12] Alternatively, the aromatic rings can be bridged or fused into folded structures that present a helical chirality.[13]

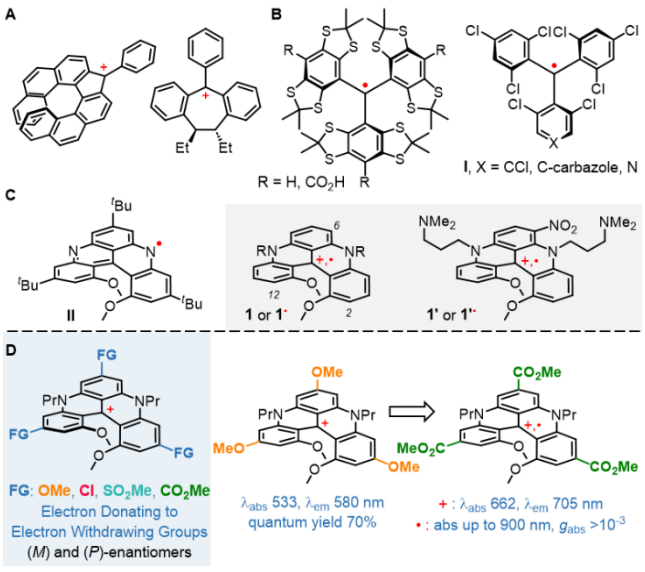

Figure 1. Examples of chiral triaryl methyl cations (**A**) [12c, 13a] and neutral radicals (**B**).[7d, 8d, g, h, 9a, 11a] Previous phenalenyl radical [14] and dimethoxyquinacridine cations and radicals (**C**).[15] This work (**D**): triple *para*-functionalized cations and neutral radicals of enantiopure diaza [4]helicenes.

Scheme 1. Enantiospecific synthesis of triple *para*-functionalized [4]helicenes ((*P*) enantiomers shown)[i]

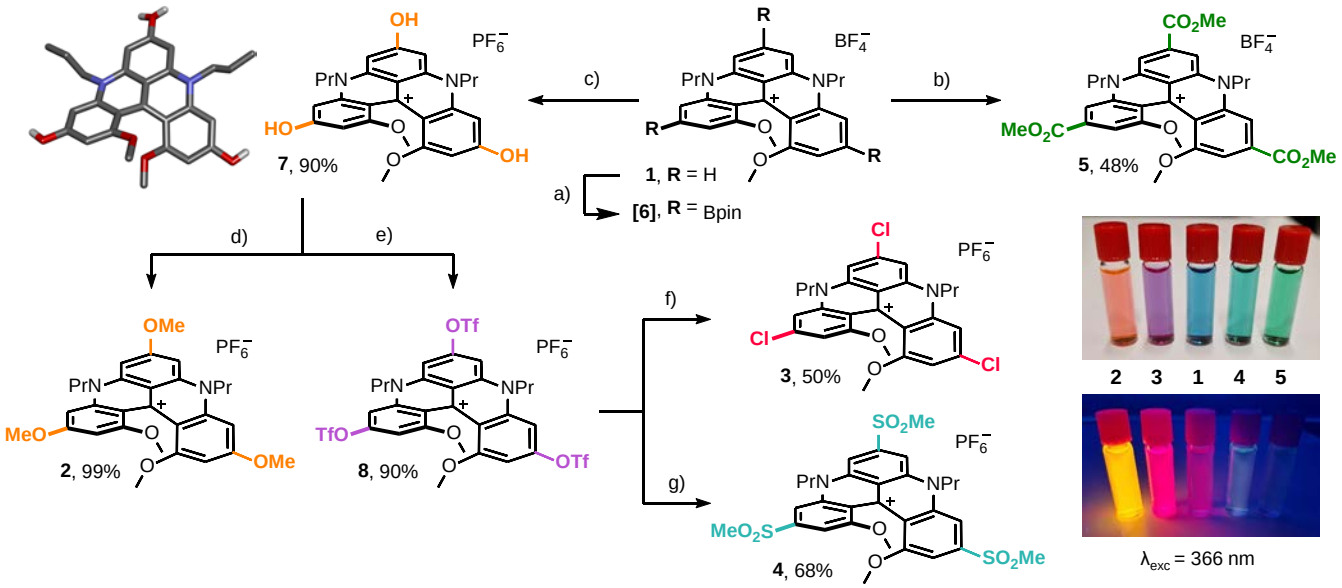

[i]Conditions: a) $[Ir(cod)OMe]_2$, tmphen, B_2pin_2, dry THF, 80 °C, 16 h; b) $Pd(OAc)_2$, PPh_3, PBQ, CO, THF:MeOH, 60 °C, 20 h; c) 1. H_2O_2 (aq), NaOH, THF, RT, 16 h, 2. anion metathesis with KPF_6 (aq); d) MeI, Cs_2CO_3, DMF, RT, 16 h; e) Tf_2O, Et_3N, CH_2Cl_2, –78 → 0 °C, 2 h; f) nBu$_4$NCl, DMF, 80 °C, 1.5 h; g) $NaSO_2Me$, MeCN, 50 °C, 16 h. Top left: X-ray crystallographic structure of **7**. Counterion and most hydrogen atoms omitted for clarity; OH group at position 7 with a local disorder for the H-atom. Bottom right: acetonitrile solutions of **1** to **5** without and with light irradiation.

At this interplay between triaryl methyl derivatives and helicenes[16] is the class of dimethoxyquinacridinium (DMQA) **1**.[17] These small [4]helicene dyes beneficiate of a high configurational stability ($\Delta G^{\ddagger}_{racem}$ ~ 42 kcal mol^{-1}).[17b] They have been used as catalysts, electrolytes in organic redox flow batteries, spin filters and bioprobes.[5e, 18] In addition, they have been proven to be good candidates for obtaining neutral radicals stable enough to be characterized.[15] To our knowledge, chiroptical properties of such neutral moieties have not been considered apart from the study by Takui, Morita and coworkers in the related phenalenyl series (Figure 1C).[14] In this example **II**, the three *tert*-butyl groups were key to achieve a good chemical stability of the radical adduct. Herein, in a new development, the preparation of a series of cationic [4]helicenes bearing triple OMe **2**, Cl **3**, SO_2Me **4**, and CO_2Me **5** groups *para* to the formally charged central carbon is presented. This substitution pattern, made possible thanks to a late-stage functionalization (LSF) strategy,[19] is achieved in 3 to 5 steps from 1,3-dimethoxybenzene. The electron-donating and electron-withdrawing groups (EDGs and EWGs) induce major blue or red shifts in the absorption and emission spectra, respectively ($\Delta\lambda_{abs}$ and $\Delta\lambda_{em}$ ±50-90 nm compared to **1**). A significant increase of fluorescence quantum yield is observed for blue-shifted emissions, with values up to 70% (580 nm, EDG=OMe, compound **2**) which is remarkable for cationic helicenes of type **1**. With triple *para*-EWGs, compounds **4** and **5**, absorption and emission properties reach far-red to NIR regions of the light spectrum. Of particular importance, neutral persistent radicals are readily afforded by mono electron reductions, under electrochemical or chemical (Cp_2Co, cobaltocene) conditions (**4**$^{\bullet}$ and **5**$^{\bullet}$). Characterization of the open-shell radicals and half-life under air was investigated by electron paramagnetic resonance (EPR) spectroscopy. These configurationally-stable radical [4]helicenes present Cotton effects at low energies (λ_{abs} ~ 700-900 nm), which are sign-inverted and enhanced by one order of magnitude compared to the parent helical cations, with absorption dissymmetry factor (g_{abs}) values above 10^{-3}. Electronic and chiroptical properties are further rationalized by time dependent (TD)DFT analysis. Unlike previous descriptions for derivatives **1** and **1'**,[15] spin densities calculations demonstrate a full delocalization of the unpaired spin over the helical core.

RESULTS AND DISCUSSION

Synthesis of 2 to 5. As mentioned earlier, dimethoxyquinacridinium (DMQA) derivatives **1** are synthetized in two steps from 1,3-dimethoxybenzene. Gram scale resolution of *rac*-**1** into the corresponding (*M*) and (*P*) enantiomers, of left-and right-handed helical configuration, is readily achieved using chiral anions or auxiliary approaches.[17] Recently, the properties of cations **1** have been modulated by regioselective introduction of substituents, usually by electrophilic aromatic substitutions (S_EAr) favoring C-H functionalization *meta* to the formal (central) positive charge.[20] Introduction of *para*-substituents onto DMQA can only be realized, unlike the related triangulenium series,[21] by LSF. In fact, inspired by the work Matsuda and coworkers,[22] it was recently shown that direct C-H trisborylation of *rac*-,

(*P*)- and (*M*)-**1** can be performed under Hartwig's methodology (B_2pin_2 with catalytic [Ir(cod)OMe]$_2$ and tmphen).[23] The regioselectivity is favored by the lower steric demand of *para* with respect to *meta* positions. Experimentally, isolation of **6** is not feasible but this intermediate was used for further Suzuki-Miyaura cross-couplings.[24] The introduction of aryl groups brought about the improvement of fluorescence quantum yields and lifetimes, while showing only moderate effect on the energy range of absorption and emission.

For the introduction of strong EWGs and EDGs linked directly to the core helical structure, several options were then considered. On one hand, Pd^{II}-catalyzed alkoxycarbonylations were achieved following conditions similar to that reported (Scheme 1, path b).[25] Usually, these arylboronate transformations are carried out in MeOH solution. Herein, due to the sensitivity of the tris(BPin) intermediate, the crude THF solution of *rac*-**6** was directly added to $Pd(OAc)_2$, PPh_3 and *para*-benzoquinone (PBQ). After bubbling carbon monoxide for 10 minutes, MeOH was added last to afford the desired tris ester *rac*-**5**. Experimentally, it was found that an increase of PBQ (up to 3 equiv) was favorable,[26] and compound **5** carrying three EW ester groups was isolated in 48% yield. Considering that product *rac*-**5** results, in a one-pot process, from three regioselective borylations followed by three alkoxycarbonylations, such a yield is actually quite noticeable.

On the other hand, by adding H_2O_2 (10 equiv) and NaOH (1 equiv) to crude reaction mixtures of **6**, an effective formation of tris hydroxylated **7** was achieved (path c). Compound **7**, as a tetrafluoroborate BF_4^- salt, was found to be scarcely soluble in solvents other than methanol, acetone and acetonitrile. To help its isolation, anion exchange metathesis to hexafluorophosphate PF_6^- and extraction in EtOAc were realized. **7** was isolated in excellent 90% yield after chromatography. As expected from previous reports of triangulenium analogues,[21a] compound **7** is sensitive to pH (Figure S13), as the various hydroxyl groups are easily deprotonated in solution, which was not ideal for further studies. Hence, compound **2** containing three methoxy groups was prepared in 99% yield by alkylation with methyl iodide under basic conditions (Scheme 1, path d).

Compound **7** turned out to be a versatile synthetic platform, via the formation of triflate analogue **8**, which can be isolated and characterized (Scheme 1, path e). In solution, it still hydrolyses over time and must be used rapidly in further reactions. This derivative is in fact susceptible to

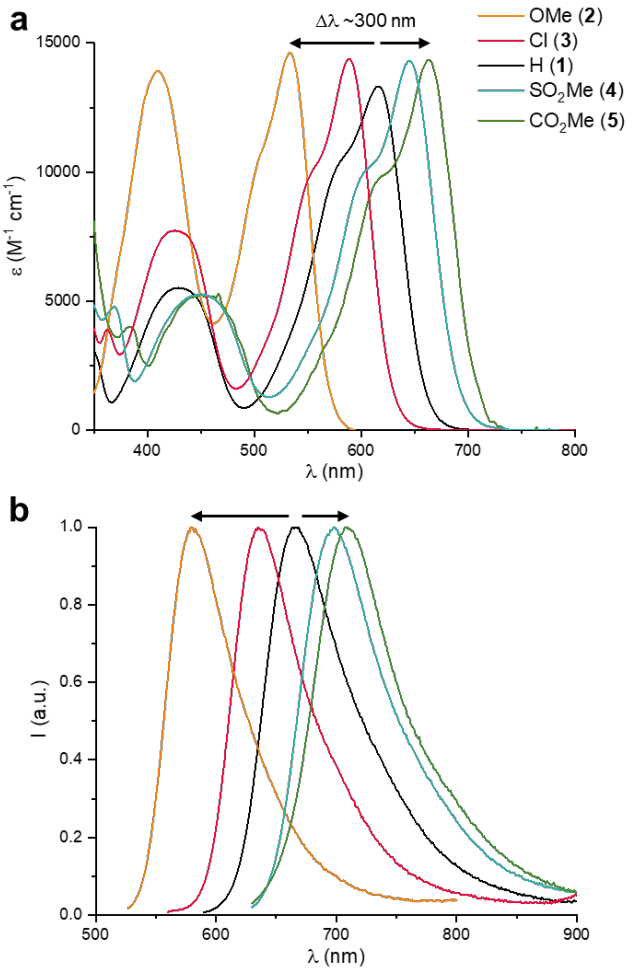

Figure 2. a) Absorption and b) normalized emission spectra of compound **1** (black), **2** (orange), **3** (fuchsia), **4** (light blue) and **5** (green) in air-equilibrated acetonitrile at RT with concentrations $1{\cdot}10^{-5}$ to $5{\cdot}10^{-6}$ M.

Table 1. Photophysical properties of triple *para*-functionalized cationic [4]helicenes in acetonitrile.

Compound[a]	λ_{max} (nm)	ε (M^{-1} cm^{-1})	λ_{em} (nm)	Stokes shift (cm^{-1})	Φ_f (%)[b]	τ (ns)[h]	k_r (10^6 s^{-1})[i]	k_{nr} (10^6 s^{-1})[l]	Optical energy gap E_{oo} (eV)
OMe (**2**)	533	14610	580	1521	70[c]	15.7	45	19	2.24
Cl (**3**)	588	14370	635	1258	40[d]	11.4	35	53	2.03
H (**1**)	616	13140	667	1242	14[e,f]	5.6[f]	25	154	1.94
SO_2Me (**4**)	645	14310	698	1177	7[g]	3.0	23	310	1.85
CO_2Me (**5**)	662	14550	705	922	5[g]	2.0	25	480	1.81

[a] Concentrations $1{\cdot}10^{-5}$ to $5{\cdot}10^{-6}$ M; [b] Φ_f estimated error = ± 10%; [c] rhodamine B (Φ = 70% in MeOH); [d] cresyl violet perchlorate (Φ = 58% in EtOH); [e] oxazine 170 perchlorate (Φ = 58% in EtOH); [f] ref 24; [g] oxazine 1 perchlorate (Φ = 15% in EtOH); [h] λ_{exc} = 400 nm; [i] $k_r = \Phi_f/\tau$; [l] $k_{nr} = (1-\Phi_f)/\tau$.

multiple nucleophilic aromatic substitutions (S_NAr) promoted by (i) the leaving group ability of TfO^- moieties and (ii) the positive charge in *para* to the triflates. In fact, compound **8** reacted with nBu$_4$NCl and NaSO$_2$Me to form compounds **3** and **4**, in 50 and 68% yields respectively (Scheme 1, path f and g). All these reactions were performed in racemic series but also enantiospecifically (50-350 mg scale) giving identical overall results for the (*M*) or (*P*) enantiomers of products **2** to **5**.

Photophysical and Electrochemical Properties. With compounds **2** (OMe), **3** (Cl), **4** (SO$_2$Me) and **5** (CO$_2$Me) in hand, care was taken to study the effect of the newly introduced groups on the physico-chemical properties of the helical core. Absorption and fluorescence properties were studied in acetonitrile at room temperature (Figure 2). The core structure **1**, used as a reference, presents a relative broad absorption band with maximum at 616 nm and an emission at 667 nm with fluorescence quantum yield (Φ_f) of 14% (Table 1).[24] Upon the introduction of good EDGs (OMe) in *para* position to the formal positive charge, a strong hypsochromic shift occurs with compound **2** having absorption and emission maxima at 533 nm and 580 nm, respectively. Also, a noticeable increase in the molar extinction coefficient (ε) of the second absorption band at 410 nm is observed (Figure 2). Most interestingly, compound **2** is strongly fluorescent with a relatively long lifetime (15.7 ns) and Φ_f of 70%, which is, to the best of our knowledge, the highest value obtained for cationic [4]helicene derivatives **1** or **1'**. Unprotected analogue **7** displays very similar optical properties in acidic conditions (Table S1, Figures S14-S23), confirming the effect of hydroxyl groups as EDGs. On the other hand, compounds **4** and **5**, bearing strong EWGs, SO$_2$Me and CO$_2$Me, are red-shifted in absorption and emission, with compound **5** emitting in the far red at 705 nm. Their Φ_f are lower compared to parent helicene **1**, consistently with the energy gap law (Table 1). More peculiar is the case of compound **3**. Its absorption and emission spectra are blue-shifted compared to parent **1** and the fluorescent quantum yield Φ_f is enhanced to 40%, in agreement with a behavior associated for EDGs (Table 1). Such an assumption must be taken with a pinch of salt. In fact, investigations of electrochemical and computational data will show that the chlorine atoms also act as inductive EWGs (*vide infra*). The rates of radiative decay (k_r) for compounds **1** to **5** are reported in Table 1. Investigation of their relation with the ε value and the cube of the emission frequency (ν_{em}^3) shows a linear trend (Figure S24 and Table S2), as predicted by the Strickler-Berg equation ($k_r \propto \varepsilon{\cdot}\nu_{em}^3$).[27] On the whole, the LSF strategy has allowed for an extensive tuning of the photophysical properties as these triple *para*-functionalized helicenes vary from poor to very good fluorophores (Φ_f 5 to 70%) with the lowest energy absorption (S_0-S_1) and emission bands spanning a range of 300 nm (Figure 2).

At this stage, the chiroptical properties of the (*M*) and (*P*) enantiomers of compounds **2**, **3**, **4** and **5** were studied in acetonitrile. The UV-vis electronic circular dichroism (ECD) and circularly polarized luminescence (CPL) spectra show a mirror image relationship for pairs of enantiomers and are reported in the Supporting Information (Figures S3-S12). As for parent DMQA **1**, the *para*-functionalized derivatives present pronounced ECD bands in the UV domain with $|\Delta\varepsilon|$~50-100 M^{-1} cm^{-1} and more modest signatures (< 10 M^{-1} cm^{-1}) at low energies > 600 nm with absorption dissymmetry factors (g_{abs}) of $|1\text{-}2|{\cdot}10^{-4}$.[28] While the ECD spectra of compounds **4** and **5** closely resemble that of compound **1** throughout the UV-vis range, marked differences can be noticed in the spectra of **2** and **3**, at both high and low energies (Figures S5-S7). The most noticeable difference can be seen above 500 nm, in the ECD signature corresponding to the lowest energy absorption band. In fact, unfunctionalized derivative **1** displays two Cotton effects with the same sign between 500–700 nm (λ_{max} 616 nm); (*M*) and (*P*) enantiomers have negative and positive bands, respectively. On the other hand, derivatives **2** and **3**, functionalized with electron rich moieties, present ECD spectra with an inversion of sign within this 500–700 nm region (Figures S5 and S7). This was already the case for *para*-tris(arene) derivatives previously reported.[24] Overall, all (*M*) and (*P*) enantiomers display negative and positive signs for the lowest-energy ECD band, respectively. Then, in relation to these results, negative and positive CPL signals were obtained for the (*M*) and (*P*) enantiomers of all derivatives **2** to **5**. Overall, these triple *para*-functionalized adducts present modest g_{lum} values around $|1\text{-}4|{\cdot}10^{-4}$ (see SI), which are consistent with those of g_{abs} of the most red-shifted ECD band. This similarity in dissymmetry factors is generally observed for helicenes for which the geometries of the ground and emitting excited states are comparable.[29] While the measured CPL signals of these new compounds remain low, thanks to the strongly enhanced fluorescence of compounds **2** and **3**, CPL brightness (B_{CPL}) values of 0.5 and 0.4 M^{-1} cm^{-1} are obtained, doubling that of simple cationic [4]helicene **1** (B_{CPL} 0.2 M^{-1} cm^{-1}).[30]

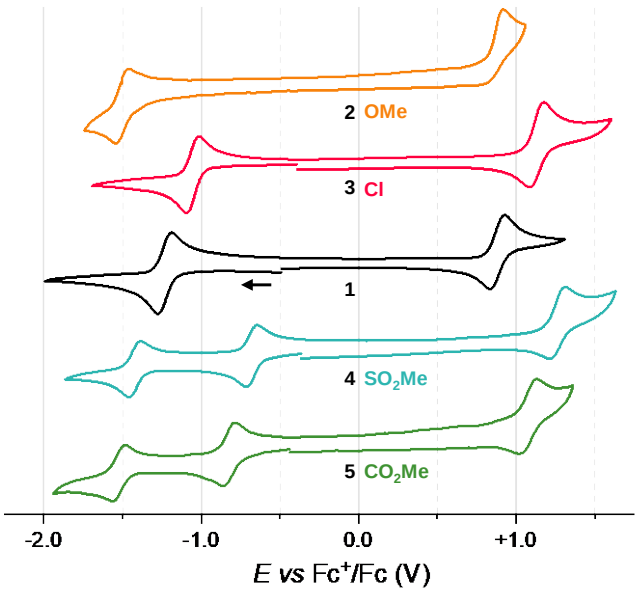

Figure 3. Cyclic voltammetry curves of **1** (black), **2** (orange), **3** (fuchsia), **4** (light blue) and **5** (green) recorded at Pt electrode (Ø = 3 mm, ν = 0.1 V/s) with concentration $5{\cdot}10^{-4}$ M in dry acetonitrile under inert atmosphere using $[n\mathrm{Bu_4N}][\mathrm{PF_6}]$ 10^{-1} M as supporting electrolyte. The arrow indicates the direction of the scan (negative potential first).

Table 2. Electrochemical data of triple *para*-functionalized cationic [4]helicenes.[a]

Compound	$E_{1/2}^{red}$ (ΔE_p)	$E_{1/2}^{ox}$ (ΔE_p)	Electrochemical energy gap (eV)
OMe (**2**)	−1.50 (72)	+0.92[c]	2.25
Cl (**3**)	−1.05 (73)	+1.12 (83)	2.05
H (**1**)	−1.23 (75)	+0.88 (90)	1.98
SO_2Me (**4**)	−0.68 (63) −1.42 (71)[b]	+1.26 (87)	1.82
CO_2Me (**5**)	−0.82 (76) −1.53 (68)[b]	+1.08 (83)	1.74

[a] $E_{1/2}$ (V, *vs* Fc^+/Fc) and peak-to-peak separations (ΔE_p in mV) for the redox processes exhibited at Pt electrode by [4]helicenes **1-5** ($5{\cdot}10^{-4}$ M) in dry acetonitrile with $[n\mathrm{Bu_4N}][\mathrm{PF_6}]$ 10^{-1} M as supporting electrolyte (measured with ν = 0.1 V/s); [b] reversible second one-electron reduction values; [c] peak potential value for irreversible processes.

Then, the electrochemical properties of **2**, **3**, **4** and **5** were studied by cyclic voltammetry (CV) in acetonitrile under inert atmosphere (Figure 3). Compound **1** was again used as a reference to investigate the influence of the newly added substituents. As reported, **1** displays an electrochemically and chemically reversible reduction at −1.23 V (ΔE_p = 75 mV and i_b/i_f ~1, with scan rate 0.1 V/s, Table 2 and S3) and an electrochemically quasi-reversible oxidation at +0.88 V (*vs* Fc^+/Fc).[15b] In previous studies, oxidative processes were mostly impacted by the mono-introduction of EDGs and EWGs in position 6 of the helical core.[31] In contrast, with the triple *para*-functionalization, processes are most influenced in the reduction regime (negative potentials, Figure 3). The electron-rich methoxy groups of compound **2** render the one-electron reduction more difficult and chemically less reversible (i_b/i_f = 0.8, with scan rate 0.1 V/s, Table S3), while the oxidation process remains at about the same potential but completely loses its reversibility. Alternatively, thanks to the EW character of the CO_2Me and SO_2Me groups, derivatives **4** and **5** are easier to reduce than unfunctionalized **1** and present two one-electron reduction processes exhibiting both electrochemical and chemical stability (ΔE_p ~70 mV and i_b/i_f >0.95, with scan rate 0.1 V/s, Table S3). A first reduction is visible at −0.82 V and −0.68 V and a second one at −1.53 V and −1.42 V, for **4** and **5** respectively (Table 2). Also, the oxidation processes (one-electron, quasi-reversible) occur at formal potentials ($E_{1/2}^{ox}$) higher than that of **1** as expected from EWGs. Of note, sulfones present a stronger EW character than carbonyl ester groups. This can be observed in the larger upward shift for both reduction and oxidation processes of **4** compared to **5**. These results will be later corroborated by DFT calculations of the frontier molecular orbitals. Finally, in opposition with the optical properties suggesting a general ED behavior for the chlorine atoms, the CV traces of tris(Cl) **3** presented more similarities with those of **4** and **5** bearing EWGs (Table 2). Clearly, in the present case, the Cl atoms behave both as σ-accepting and π-donating groups. Consequently, and for this derivative only, the substituents have a stronger influence on the oxidation rather than the reduction processes; a behavior that will be better rationalized with the help of the molecular orbital analysis. Overall, a good agreement is found between electrochemical energy gaps (E_{onset}^{ox}–E_{onset}^{red}) and optical ones of all derivatives (Tables 1 and 2). Additional electrochemical data (*i.e.*, potentials of the irreversible second one-electron reductions of **1**, **2** and **3**) are reported in the Supporting Information, Table S3.

The observed optical and electrochemical properties can be rationalized by studying the molecular orbitals (MOs). MOs were investigated by DFT calculations truncating, for computational ease, the *N*-propyl sidechains to *N*-methyl (Figures 4 and S58). Generally, an opposite effect on properties is observed upon introduction of *para*-EDGs or -EWGs, compared to that previously observed for *meta*-substituents *i.e.*, at position C-6 of the helical core (Figure 1).[31,32] Dewar's perturbation molecular orbital theory is then a valuable tool to rationalize the observed evolution, as shown for related triangulenium cations.[33] In fact, while HOMO and LUMO orbitals on compound **1** present nodes and localizations at the *para* positions, respectively (Figure 4), the reverse situation occurs at *meta* positions. Therefore, while *meta* functionalization impacts the HOMO orbital more strongly, herein, *para*-substituents influence more significantly LUMO orbitals, with EDGs bringing about a destabilization (*i.e.*, blue-shift and lower $E_{1/2}^{red}$) and EWGs a stabilization (*i.e.*, red-shift and higher $E_{1/2}^{red}$).

Consistently, as shown in Figure 4, for all the compounds, the distribution of the HOMO remains mostly on the helical scaffold with little extension toward the added groups. On the other hand, LUMO orbitals are localized at the substituted carbons, and generally involve the introduced atoms or functional groups. The frontier molecular orbitals of **2** are at higher energy with respect to **1** and a stronger destabilization of the LUMO causes the blue shift of the red-most absorption band and emission. Instead, MOs of compounds **4** and **5** are stabilized with respect to **1**, with SO_2Me being a stronger EWG than CO_2Me,[34] but giving overall a bigger energy gap between HOMO and LUMO. As specified before, the introduction of chlorine atoms on the helical core has an effect that is out of trend with respect to the other derivatives. While the chlorine atoms act as inductive EWGs in stabilizing the frontier MOs, the energy band gap is higher than that of **1** resulting in a blue shift in the optical properties. In fact, these three atoms have a stronger stabilizing effect on the energy of the HOMO *vs* the LUMO orbitals. The absolute energy values in vacuum of the HOMO and LUMO orbitals for compounds **1** to **5** were derived from electrochemical data and are reported in the Supporting Information (Table S4).

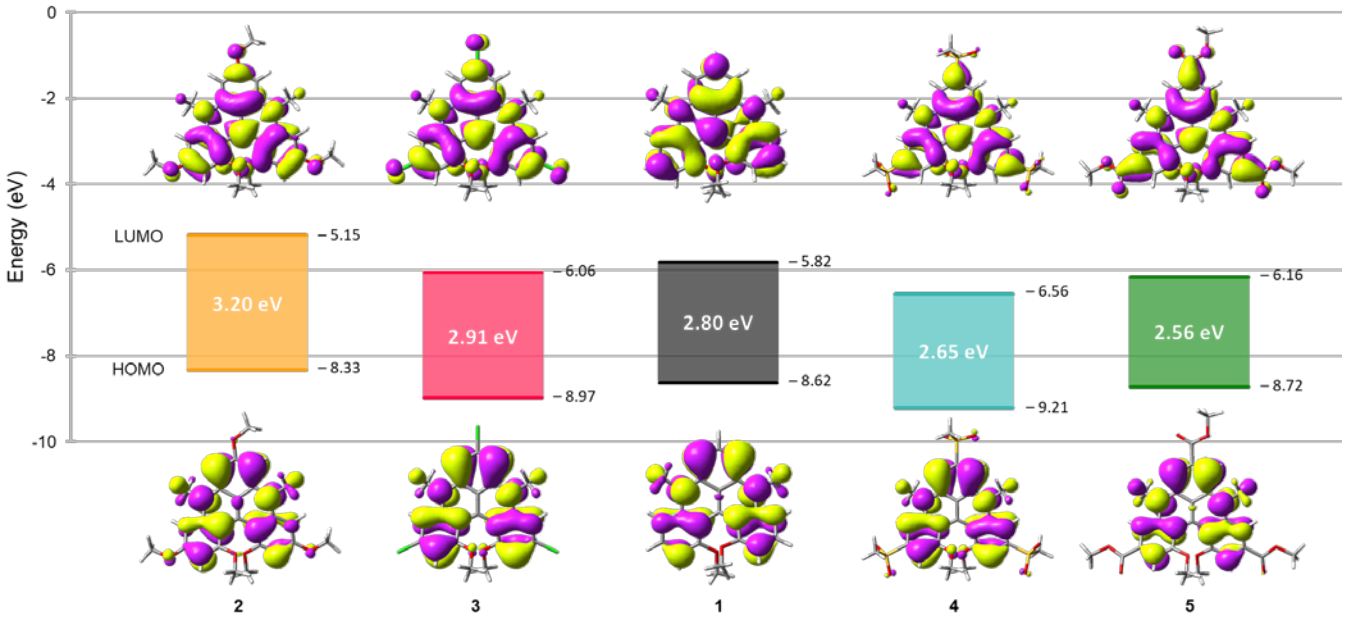

Figure 4. HOMO and LUMO Kohn-Sham orbitals and relative energies (eV) computed by DFT with B3LYP/def2-TZVP//B3LYP/6-31+G(d,p) for truncated NMe analogs of compounds **1**, **2**, **3**, **4** and **5**.

In conclusion for this part, as confirmed by electrochemical measurements and DFT calculations, introduction of three EWGs in *para* to the formal positive charge causes a stabilization of LUMO orbitals with respect to unfunctionalized **1**. As a result, one-electron reduction processes are more favored. Derivatives **4** and **5** are the easiest to reduce, with $E_{1/2}^{red}$ higher than all previously reported values for cationic diaza [4]helicenes (Table 2).[31] This data prompted us to investigate the formation and stability of neutral radicals obtained by mono reduction of the newly synthetized compounds.

Electrochemical and Chemical reduction - Neutral Radicals. Organic neutral radicals are open-shell molecules with an unpaired electron forming a singly occupied molecular orbital (SOMO). Such derivatives are usually reactive but specific skeletal properties can be considered to generate persistent or stable organic radicals. For instance, shielding reactive positions with bulky substituents and/or increasing the spin delocalization over large conjugated skeletons are favorable strategies.[2b, e] As mentioned earlier, polychlorinated trityl radicals are among the most stable carbon radicals. Their stability is traced to (i) their electron deficiency, (ii) functionalized *para* positions and (iii) central spin-bearing sp^2 carbon that is sterically and chemically shielded by the twisted phenyl rings and multiple chlorine atoms.[35] Further, many structural variations can be made using principally modifications at *para* positions.[8g, 36] Some of the parameters favoring higher stability, such as the introduction of bulky *para* substituents, are also important for extended triarylmethyl, triangulene and helicene radical structures.[14, 37] In the following paragraphs, single-electron reductions of cationic helicenes **2** to **5** are investigated with a focus on the reversibility of the redox process (Equation 1), the chemical stability of the derived neutral radicals **2**• to **5**• and, when possible, the chiroptical properties.

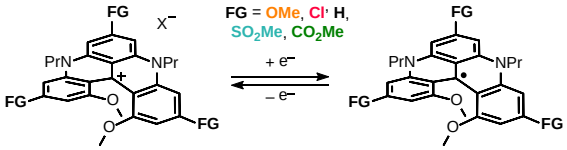

(1)

Initial studies started with investigation of compound **1** and its radical state obtained upon mono electron reduction (**1**$^{\bullet}$), a species reported for the first time in 2014 by Laursen and coworkers.[15b] In the article, the reduction of **1** in acetonitrile led to the formation of central adducts (**1**-H and **1**-CH_2CN) due to the low stability of radical species **1**$^{\bullet}$ in this solvent. The absorption spectrum of **1**$^{\bullet}$, obtained by electrolysis under strictly anaerobic conditions in inert benzonitrile as solvent, was nonetheless reported. Higher energy and lower molar extinction coefficient ε were noted for the first absorption band of **1**$^{\bullet}$, compared to the parent carbocation **1**. A localization of radical on the central carbon with consequential loss of conjugation was hence hypothesized. Here, to complement this study,[15b] the *in situ* spectroelectrochemistry of **1** is presented; the results being used as benchmark in comparison with new *para*-substituted compounds **2** to **5**.

First, *in situ* spectroelectrochemistry was performed for compounds **1** to **5** tracking the formation of the neutral radical species. UV-vis absorption spectra were recorded during a slow cyclic voltammetry scan (ν = 0.5 mV/s), using an optically transparent thin-layer electrochemical (OTTLE)[38] cell in acetonitrile solutions with [$n$$Bu_4N$][$PF_6$] 10^{-1} M as supporting electrolyte.

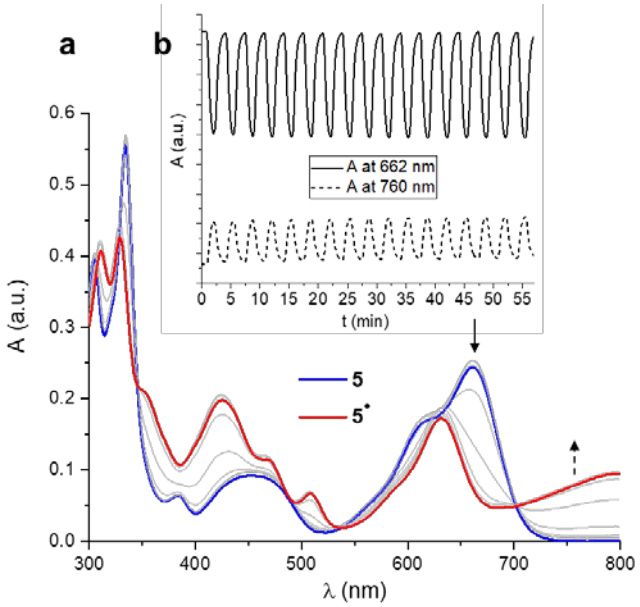

Figure 5. Spectroelectrochemical studies performed in an OTTLE cell of **5** in dry acetonitrile (C *ca.* $4.5{\cdot}10^{-4}$ M, [$n$$Bu_4N$][$PF_6$] 10^{-1} M as supporting electrolyte). a) UV-vis spectral changes recorded every 2 minutes during a CV scan between 0.0 and −0.6 V (*vs* Ag wire pseudo-reference electrode; ν = 0.5 mV/s). Only the reduction process is shown with spectra of **5** in blue and **5**$^{\bullet}$ in red; b) absorption changes at λ = 662 nm (full line) and λ = 760 nm (dotted line) recorded every 2 seconds during 17 successive CV cycles (ν = 10 mV/s).

For **1**, changing the potential between 0.0 and −0.95 V (*vs* Ag wire pseudo-reference electrode), two absorption maxima appear upon reduction at 390 and 560 nm corresponding to the formation of **1**$^{\bullet}$ as previously reported (Figure S25).[15b] For this transformation, the isosbestic points are not well defined as **1**$^{\bullet}$ undergoes degradation and, following the reverse oxidation process to **1**, only partial reversibility could be observed. The formation and reoxidation of **1**$^{\bullet}$ were also investigated at a single wavelength (λ = 614 nm) during multiple CV cycles with scan rate 10 mV/s (Figure S26). Quicker CV scan rates allowed to perform multiple reduction/oxidation cycles with only moderate degradation. Nevertheless, after each cycle, the absorption intensity of **1** at 614 nm is not fully recovered. Identical spectroelectrochemical investigations were performed for compounds **2**, **3**, **4** and **5**. Upon reduction, compounds **2** and **3** showed spectral changes similar to **1**; the spectrum of **3**$^{\bullet}$ differing by the presence of a broad low intensity absorption band centered at 700 nm. For both compounds **2** and **3**, only partial reversibility is again observed after reoxidation (Figures S27 and S29), indicating a lack of persistence of the neutral radical species. Performing multiple redox cycles at a faster rate, **3** did not show significant change in the absorption intensity (Figure S30) while important modifications were visible already after a few cycles for **2** (Figure S28). Due to its low stability, neutral radical **2**$^{\bullet}$ was not investigated further. Most interesting results were obtained with compounds **4** and **5** bearing *para*-EWGs, presenting good to excellent persistence of the corresponding neutral radicals (Figures S29-S32). Spectroelectrochemistry reveals in the absorption spectra of **4**$^{\bullet}$ and **5**$^{\bullet}$, between 400 and 500 nm, three overlaying peaks and a single one around 600 nm. Of importance, both spectra extend toward the NIR with moderately intense bands centered at 750 and 800 nm, respectively (Figure S31 compound **4** and Figure 5a compound **5**). For compound **5**$^{\bullet}$, this lowest energy absorption band reaches 900 nm (Figure 6 and S50). For the reduction process of both **4** and **5**, several isosbestic points are present between 300 and 800 nm. Those are perfectly maintained for compound **5** during the reverse oxidation process indicating the stability of **5**$^{\bullet}$ in the spectroelectrochemistry time scale (Figure S33). Also, over multiple redox cycles in rapid succession, stability is maintained for both **4** (Figure S32) and **5** (Figure 5b) with no visible loss of absorption intensity. Additionally, to complement the experiments, DFT calculations were performed for all neutral radical derivatives (Figure S69). Large differences can be noticed in the MOs from **2**$^{\bullet}$ and **5**$^{\bullet}$ with (i) very high energies for LUMO and LUMO+1 in the presence of EDGs (**2**$^{\bullet}$) and (ii) strong SOMO stabilization with the introduction of EW substituents in **4**$^{\bullet}$ and **5**$^{\bullet}$. These theoretical data reflect the experimental reactivity: a persistence for **4**$^{\bullet}$ and **5**$^{\bullet}$ and a lack of stability for **2**$^{\bullet}$, **3**$^{\bullet}$, and unsubstituted **1**$^{\bullet}$.

Then, *rac*-, (*M*) and (*P*) samples of **1**, **4** and **5** were utilized in bulk experiments.[39] Electrolysis was performed at fixed negative potentials, defined by previous CV studies, and full conversion of the cationic helicenes to the neutral radicals was obtained. Aliquots of the enantiopure compounds were taken to record absorption and ECD spectra. Firstly, for **1**$^{\bullet}$, its bulk formation displayed signs of degradation already during electrolysis, before the complete reduction of **1** could be achieved. After electrolysis of **1**, the ab-

sorption spectrum presented intensities lower than expected in view of previous experiments (Figure S36). Furthermore, ECD spectra of (*M*)-**1**$^{\bullet}$ and (*P*)-**1**$^{\bullet}$ were not perfect mirror image to each other. Likely, substantial parts of **1**$^{\bullet}$ in each sample reacted to form other products such as **1**-H and **1**-CH_2CN.[15b] These solutions were then electrolyzed at positive potentials to enforce the opposite oxidative process and assess the chemical reversibly in bulk transformations. In this context, different delays in reoxidation of (*M*) and (*P*) batches accounted for different spectral outcome (Figure S35). This was not the case for compounds **4** and **5**. In fact, samples showed outstanding stability to bulk electrochemical reduction and very good reversibility upon reoxidation (Figures S38 and S43). Furthermore, absorption spectra of **4**$^{\bullet}$ and **5**$^{\bullet}$ monitored during 15 h under inert atmosphere demonstrated only small changes mostly attributed to minor reoxidation to cationic **4** and **5** (Figures S40-S42 and S45-S47). Overall, tris ester **5**$^{\bullet}$ shows better stability than tris sulfone **4**$^{\bullet}$. Thanks to the enhanced persistence, chiroptical investigations were also carried out (Figure 6).

For radical species **4**$^{\bullet}$ and **5**$^{\bullet}$, ECD signatures recall the features appearing in the electronic absorption spectra (Figure 6). Multiple ECD bands are present across the whole spectral range with $|\Delta\varepsilon|$ ~5-40 $M^{-1}\,cm^{-1}$. Of note are the Cotton effects corresponding to the lowest energy absorption band, ranging from 680 to 800 nm for compound **4**$^{\bullet}$ and 700 to 900 nm for **5**$^{\bullet}$. These ECD signatures at low energies present absorption dissymmetry factors above 10^{-3} (g_{abs} at λ_{max} of $+1.5/-1.3\cdot10^{-3}$ for **4**$^{\bullet}$ and $+1.1/-1.3\cdot10^{-3}$ for **5**$^{\bullet}$), showing a 10-fold increase compared to the relative parent carbocations. Also, these transitions present positive and negative values for the (*M*) and (*P*)-enantiomers, respectively; that is, a sign inversion of the low energy ECD signals in comparison to **4** and **5**.[40] Good agreement between experimental and computed ECD spectra was obtained by TDDFT calculations for both radical compounds (Figures S75 and S77).[41] Transition analysis revealed that the lowest energy ECD band is composed mostly by the SOMO → LUMO transition with a contribution from the HOMO → SOMO (Figures S76 and S78); this analysis explaining the sign inversion for the low-energy Cotton effect (ECD) between cations and radicals. From MO analysis, the open-shell nature of the radical has been established without requiring establishing a SOMO-HOMO inversion which is important in other molecular systems.[8h, 42]

Finally, a focus was given to the reduction of **4** and **5** using a chemical reagent. Based on the $E_{1/2}^{red}$ values (> –0.9 V), cobaltocene was selected as a suitable reductant ($[CoCp_2]^+$ → $[CoCp_2]$ E = –1.3 V *vs* Fc^+/Fc).[43] It was also selected as it would not induce a second reduction to the carbanionic species (E <–1.4 V). The reduction experiments were performed in dry acetonitrile under inert atmosphere adding only a moderate excess of $CoCp_2$. Formation of the radicals was monitored by UV-vis absorption spectra (Figures S48 and S50).

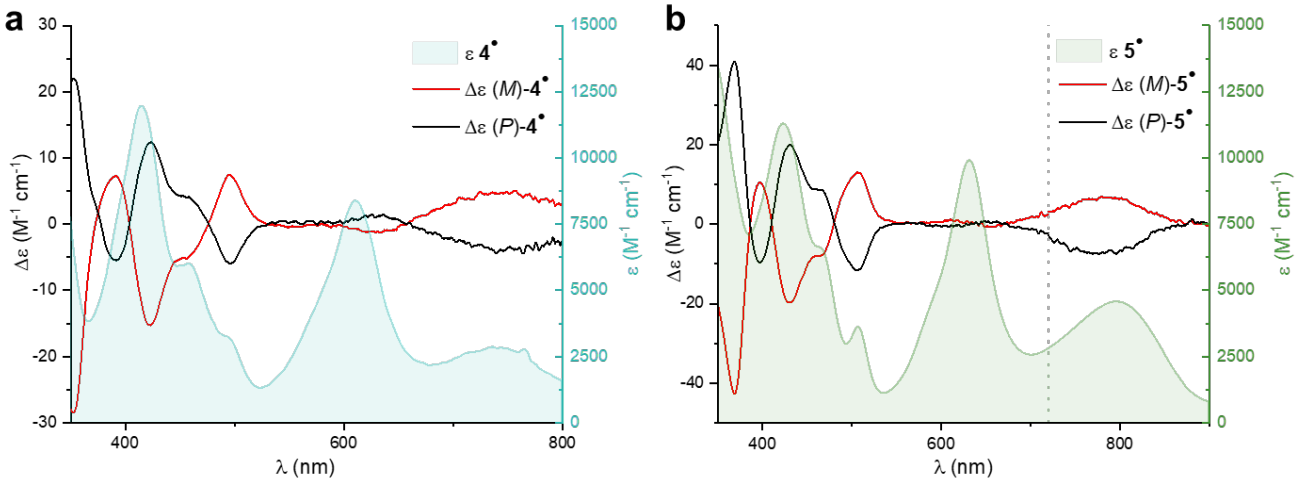

Figure 6. ECD spectra (red (*M*) and black (*P*) lines) and absorption spectra (underlying filled curve) in the UV-vis-NIR range of a) **4**$^{\bullet}$ and b) **5**$^{\bullet}$ obtained by electrochemical reduction in dry acetonitrile (C *ca.* $4.5\cdot10^{-4}$ M, $[n\text{Bu}_4\text{N}][PF_6]$ 10^{-1} M as supporting electrolyte) using a quartz cuvette, 0.1 cm optical path, sealed under Ar. The absorptions of the solvent and the supporting electrolyte have been subtracted. The vertical dotted line at 720 nm (**5**$^{\bullet}$) separates the ECD spectrum fragments measured on two different instruments.

Perfect agreement was observed between spectra of compound **5**$^{\bullet}$ obtained by chemical reduction and those achieved through electrochemistry (Figure S53), whereas the absorption of **4**$^{\bullet}$ produced with $CoCp_2$ showed lower intensity, although maintaining identical spectral features (Figure S49).[44] To evaluate the persistence of **5**$^{\bullet}$, changes in the absorption spectrum after chemical reduction were monitored in time. As observed before, under inert atmosphere, significant changes can be noticed only after 15 h (Figure S51a). Under air exposure, the spectrum of **5**$^{\bullet}$ undergoes faster modifications (Figure S51b). Nonetheless, after 30 h, the characteristic band at 800 nm remains indicating that radical species still persists in solution. Importantly, if **5**$^{\bullet}$ is stored as a solid under inert atmosphere and dissolved again in acetonitrile, its absorption spectrum

remains mostly unchanged even after multiple days (Figure S52). These experiments point collectively to the good persistence of this helical radical.

As expected, EPR measurements confirmed the open-shell electronic nature of **4**$^{\bullet}$ and **5**$^{\bullet}$ (Figure 7). Experimental and simulated spectra of **4**$^{\bullet}$ and **5**$^{\bullet}$ are shown in Figure 7a with calculated *g*(iso) values of 2.0027 and 2.0031, respectively. Isotropic hyperfine constants were calculated for the two neutral radicals (A(iso), Table S5) and a good agreement was found between simulated and experimental spectra.[45] Notably, the absence of hyperfine features in the spectrum of **4**$^{\bullet}$ indicates that the spectral linewidth of this radical is slightly larger than that of **5**$^{\bullet}$, possibly due to the presence of several interconverting diastereomeric conformations linked to the SO_2Me moieties. The spin densities of neutral radicals **4**$^{\bullet}$ and **5**$^{\bullet}$, calculated by DFT, are delocalized over the entire π system and no pyramidalization of the central carbon is observed (Figures 7b). This important spin density delocalization, unlike previously observed for **1**$^{\bullet}$,[15a] contributes to the persistence of **4**$^{\bullet}$ and **5**$^{\bullet}$. Additionally, EPR provided a practical method to evaluate the kinetics of disappearance of radicals **4**$^{\bullet}$ and **5**$^{\bullet}$ when exposed to air. Half-life values of about 5 and 7 h were determined, respectively (Figures S55 and S57). These values are quite remarkable for measurements made in a reactive solvent such as acetonitrile.[15b,46]

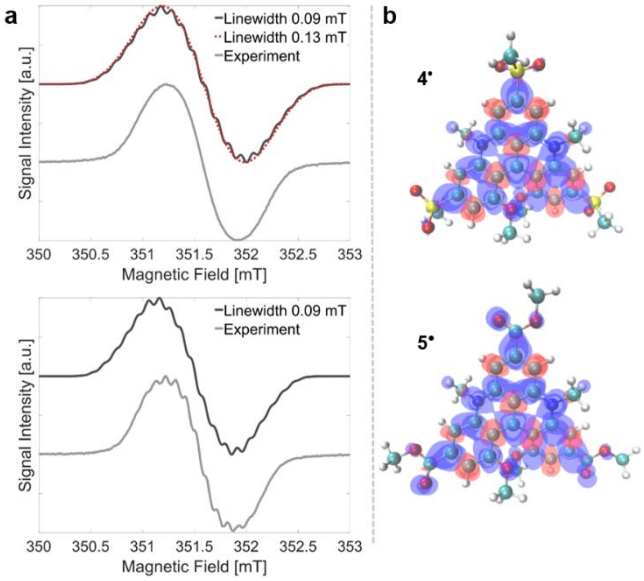

Figure 7. EPR data of **4**$^{\bullet}$ (top) and **5**$^{\bullet}$ (bottom). a) Room temperature continuous wave X-band EPR spectra obtained by chemical reduction in acetonitrile (grey, concentration *ca.* $3{\cdot}10^{-4}$ M) under inert atmosphere and simulated spectra (black, linewidth 0.09 mT or dotted red, linewidth 0.13 mT) using Easyspin. Experimental conditions are given in the supporting information. b) Spin density distribution calculated using the UKS method B3LYP/IGLO-II. Blue and red colors refer to alpha and beta spin density, respectively (isovalue 0.0004).

CONCLUSIONS

In this study, a series of enantiopure derivatives bridging triaryl methyl and helicene domains, cations and neutral radicals, have been prepared. An effective enantiospecific synthesis, using a LSF strategy, affords triple *para*-functionalized DMQA derivatives **2** to **5** in few steps from simple building blocks with good to excellent yields. The novel electron-donating and electron-withdrawing groups induce significant changes in electronic and (chir)optical properties. All cationic derivatives are luminescent, from orange to NIR regions of the light spectrum, with quantum yields up 70% which is unusual for derivatives of type **1**. With EWGs, persistent neutral radicals are readily afforded by mono electron reductions, under electrochemical or chemical (Cp_2Co) conditions; the reversibility of redox process being particularly sustainable even in bulk. The open-shell radical nature of **4**$^{\bullet}$ and **5**$^{\bullet}$ and their half-lives under air were investigated by EPR spectroscopy, revealing an important spin density delocalization which contributes to their persistence. These configurationally-stable radical [4]helicenes present Cotton effects at low energies (λ_{abs} ~ 700-900 nm), sign-inverted and enhanced by one order of magnitude compared to the parent helical cations, with g_{abs} values above 10^{-3}. DFT calculations afforded HOMO/LUMO levels in agreement with the observed spectral changes upon substitution. Thanks to these new compounds with extended electronic and optical properties, innovative applications are foreseeable that will extend the already-broad collection of uses for DMQA derivatives.

ASSOCIATED CONTENT

Supporting Information for this article is given via a link at the end of the document. It contains experimental conditions, characterizations of all new compounds, UV-Vis and fluorescence spectra, electrochemistry measurements, calculations and EPR data.

The data that support the findings of this study are openly available in yareta.unige.ch at https://doi.org/10.26037/yareta:xpcqve5xjzg23clrevo3gxw67m . It will be preserved for 10 years.

CCDC 2308535 contains the supplementary crystallographic data for this paper. These data can be obtained free of charge via www.ccdc.cam.ac.uk/data_request/cif, or by emailing data_request@ccdc.cam.ac.uk, or by contacting The Cambridge Crystallographic Data Centre, 12 Union Road, Cambridge CB2 1EZ, UK; fax: +44 1223 336033.

AUTHOR INFORMATION

Corresponding Author

Jérôme Lacour – *Department of Organic Chemistry, University of Geneva, Quai Ernest Ansermet 30, 1211 Geneva 4, Switzerland*.

Email: jerome.lacour@unige.ch

Authors

Bibiana Fabri - *Department of Organic Chemistry, University of Geneva, Quai Ernest Ansermet 30, 1211 Geneva 4, Switzerland*

Tiziana Funaioli – *Dipartimento di Chimica e Chimica Industriale, University of Pisa, Via G. Moruzzi 13, 56124 Pisa, Italy*

Lucas Frédéric - *Department of Organic Chemistry, University of Geneva, Quai Ernest Ansermet 30, 1211 Geneva 4, Switzerland*; #Present Address: Université Paris-Saclay, ENS Paris-Saclay, CNRS, 4 avenue des sciences, 91190, Gif-sur-Yvette, France

Christina Elsner – *Department of Physical Chemistry, University of Geneva, Quai Ernest Ansermet 30, 1211 Geneva 4, Switzerland*

Enrica Bordignon – *Department of Physical Chemistry, University of Geneva, Quai Ernest Ansermet 30, 1211 Geneva 4, Switzerland*

Francesco Zinna– *Dipartimento di Chimica e Chimica Industriale, University of Pisa, Via G. Moruzzi 13, 56124 Pisa, Italy*

Lorenzo Di Bari– *Dipartimento di Chimica e Chimica Industriale, University of Pisa, Via G. Moruzzi 13, 56124 Pisa, Italy*

Gennaro Pescitelli– *Dipartimento di Chimica e Chimica Industriale, University of Pisa, Via G. Moruzzi 13, 56124 Pisa, Italy*

Funding Sources

Swiss National Science Foundation 200020-184843 and 200020-207539. European Commission Research Executive Agency (Grant Agreement Number: 859752 HEL4CHIROLED H2020-MSCA-ITN-2019).

ACKNOWLEDGMENT

We thank the University of Geneva, the Swiss National Science Foundation and the European Commission Research Executive Agency for financial support. Open access funding was provided by the University de Geneva. We thank Dr Céline Besnard (University of Geneva) for the X-ray measurements, Stéphane Grass (University of Geneva) for the help in preparing synthetic materials and Prof. Eric Vauthey (University of Geneva) for giving access to the time-correlated single photon counting setup. G. P. acknowledges the CINECA award under the ISCRA initiative for the availability of high-performance computing resources and support.

ABBREVIATIONS

ECD, electronic circular dichroism; CPL, circularly polarized luminescence; LSF, late-stage functionalization; EDGs, electron donating groups; EWGs, electron withdrawing groups; CV, cyclic voltammetry; MOs, molecular orbitals; EPR, electron paramagnetic resonance.

REFERENCES

(1) (a) Arikawa, S.; Shimizu, A.; Shiomi, D.; Sato, K.; Takui, T.; Sotome, H.; Miyasaka, H.; Murai, M.; Yamaguchi, S.; Shintani, R. A Kinetically Stabilized Nitrogen-Doped Triangulene Cation: Stable and NIR Fluorescent Diradical Cation with Triplet Ground State. *Angew. Chem. Int. Ed.* **2023**, *62*, e202302714. (b) Dosso, J.; Bartolomei, B.; Demitri, N.; Cossío, F. P.; Prato, M. Phenanthrene-Extended Phenazine Dication: An Electrochromic Conformational Switch Presenting Dual Reactivity. *J. Am. Chem. Soc.* **2022**, *144*, 7295-7301. (c) Wei, H.; Hou, X.; Xu, T.; Zou, Y.; Li, G.; Wu, S.; Geng, Y.; Wu, J. Solution-Phase Synthesis and Isolation of An Aza-Triangulene and Its Cation in Crystalline Form. *Angew. Chem. Int. Ed.* **2022**, *61*, e202210386. (d) Lv, J.; Zhang, Q.; Zhong, X.; Luo, S. Asymmetric Latent Carbocation Catalysis with Chiral Trityl Phosphate. *J. Am. Chem. Soc.* **2015**, *137*, 15576-15583. (e) Nicewicz, D. A.; Nguyen, T. M. Recent Applications of Organic Dyes as Photoredox Catalysts in Organic Synthesis. *ACS Catalysis* **2014**, *4*, 355-360.

(2) (a) Quintes, T.; Mayländer, M.; Richert, S. Properties and applications of photoexcited chromophore–radical systems. *Nat. Rev. Chem.* **2023**, *7*, 75-90. (b) Ji, L.; Shi, J.; Wei, J.; Yu, T.; Huang, W. Air-Stable Organic Radicals: New-Generation Materials for Flexible Electronics? *Adv. Mater.* **2020**, *32*, 1908015. (c) Shu, C.; Zhang, H.; Olankitwanit, A.; Rajca, S.; Rajca, A. High-Spin Diradical Dication of Chiral π-Conjugated Double Helical Molecule. *J. Am. Chem. Soc.* **2019**, *141*, 17287-17294. (d) Kimura, S.; Kusamoto, T.; Kimura, S.; Kato, K.; Teki, Y.; Nishihara, H. Magnetoluminescence in a Photostable, Brightly Luminescent Organic Radical in a Rigid Environment. *Angew. Chem. Int. Ed.* **2018**, *57*, 12711-12715. (e) Ratera, I.; Veciana, J. Playing with organic radicals as building blocks for functional molecular materials. *Chem. Soc. Rev.* **2012**, *41*, 303-349. (f) Mas-Torrent, M.; Crivillers, N.; Mugnaini, V.; Ratera, I.; Rovira, C.; Veciana, J. Organic radicals on surfaces: towards molecular spintronics. *J. Mater. Chem.* **2009**, *19*, 1691-1695.

(3) (a) Kwon, G.; Ko, Y.; Kim, Y.; Kim, K.; Kang, K. Versatile Redox-Active Organic Materials for Rechargeable Energy Storage. *Acc. Chem. Res.* **2021**, *54*, 4423-4433. (b) Lee, S.; Hong, J.; Kang, K. Redox-Active Organic Compounds for Future Sustainable Energy Storage System. *Adv. Energy Mater.* **2020**, *10*, 2001445. (c) Ni, Y.; Gopalakrishna, T. Y.; Phan, H.; Kim, T.; Herng, T. S.; Han, Y.; Tao, T.; Ding, J.; Kim, D.; Wu, J. 3D global aromaticity in a fully conjugated diradicaloid cage at different oxidation states. *Nat. Chem.* **2020**, *12*, 242-248. (d) Kim, D. J.; Hermann, K. R.; Prokofjevs, A.; Otley, M. T.; Pezzato, C.; Owczarek, M.; Stoddart, J. F. Redox-Active Macrocycles for Organic Rechargeable Batteries. *J. Am. Chem. Soc.* **2017**, *139*, 6635-6643.

(4) (a) Li, F.; Gillett, A. J.; Gu, Q.; Ding, J.; Chen, Z.; Hele, T. J. H.; Myers, W. K.; Friend, R. H.; Evans, E. W. Singlet and triplet to doublet energy transfer: improving organic light-emitting diodes with radicals. *Nat. Commun.* **2022**, *13*, 2744. (b) Cho, H.-H.; Kimura, S.; Greenham, N. C.; Tani, Y.; Matsuoka, R.; Nishihara, H.; Friend, R. H.; Kusamoto, T.; Evans, E. W. Near-Infrared Light-Emitting Diodes from Organic Radicals with Charge Control. *Adv. Opt. Mater.* **2022**, *10*, 2200628. (c) Mattiello, S.; Corsini, F.; Mecca, S.; Sassi, M.; Ruffo, R.; Mattioli, G.; Hattori, Y.; Kusamoto, T.; Griffini, G.; Beverina, L. First demonstration of the use of open-shell derivatives as organic luminophores for transparent luminescent solar concentrators. *Mater. Adv.* **2021**, *2*, 7369-7378. (d) Obolda, A.; Ai, X.; Zhang, M.; Li, F. Up to 100% Formation Ratio of Doublet Exciton in Deep-Red Organic Light-Emitting Diodes Based on Neutral π-Radical. *ACS Appl. Mater. Interfaces* **2016**, *8*, 35472-35478. (e) Peng, Q.; Obolda, A.; Zhang, M.; Li, F. Organic Light-Emitting Diodes Using a Neutral π Radical as Emitter: The Emission from a Doublet. *Angew. Chem. Int. Ed.* **2015**, *54*, 7091-7095. (f) Sugawara, T.; Matsushita, M. M. Spintronics in organic π-electronic systems. *J. Mater. Chem.* **2009**, *19*, 1738-1753. (g) Wang, Y.; Wang, H.; Liu, Y.; Di, C.-a.; Sun, Y.; Wu, W.; Yu, G.; Zhang, D.; Zhu, D. 1-Imino Nitroxide Pyrene for High Performance Organic Field-Effect Transistors with Low Operating Voltage. *J. Am. Chem. Soc.* **2006**, *128*, 13058-13059.

(5) (a) Li, C.; Zhang, C.; Li, P.; Jia, Y.; Duan, J.; Liu, M.; Zhang, N.; Chen, P. Red Emissive Double Aza[7]helicenes with Antiaromaticity / Aromaticity Switching via the Redox-Induced Radical Cation and Dication Species. *Angew. Chem. Int. Ed.* **2023**, *62*, e202302019. (b) Rodríguez, R.; Naranjo, C.; Kumar, A.; Matozzo, P.; Das, T. K.; Zhu, Q.; Vanthuyne, N.; Gómez, R.; Naaman, R.; Sánchez, L.; Crassous, J. Mutual Monomer Orientation To Bias the Supramolecular Polymerization of [6]Helicenes and the Resulting Circularly Polarized Light and

Spin Filtering Properties. *J. Am. Chem. Soc.* **2022**, *144*, 7709-7719. (c) Tani, F.; Narita, M.; Murafuji, T. Helicene Radicals: Molecules Bearing a Combination of Helical Chirality and Unpaired Electron Spin. *ChemPlusChem* **2020**, *85*, 2093-2104. (d) Kasemthaveechok, S.; Abella, L.; Jean, M.; Cordier, M.; Roisnel, T.; Vanthuyne, N.; Guizouarn, T.; Cador, O.; Autschbach, J.; Crassous, J.; Favereau, L. Axially and Helically Chiral Cationic Radical Bicarbazoles: SOMO–HOMO Level Inversion and Chirality Impact on the Stability of Mono- and Diradical Cations. *J. Am. Chem. Soc.* **2020**, *142*, 20409-20418. (e) Kiran, V.; Mathew, S. P.; Cohen, S. R.; Hernández Delgado, I.; Lacour, J.; Naaman, R. Helicenes—A New Class of Organic Spin Filter. *Adv. Mater.* **2016**, *28*, 1957-1962. (f) Wang, Y.; Zhang, H.; Pink, M.; Olankitwanit, A.; Rajca, S.; Rajca, A. Radical Cation and Neutral Radical of Aza-thia[7]helicene with SOMO–HOMO Energy Level Inversion. *J. Am. Chem. Soc.* **2016**, *138*, 7298-7304. (g) Ravat, P.; Ribar, P.; Rickhaus, M.; Häussinger, D.; Neuburger, M.; Juríček, M. Spin-Delocalization in a Helical Open-Shell Hydrocarbon. *J. Org. Chem.* **2016**, *81*, 12303-12317. (h) Pop, F.; Auban-Senzier, P.; Canadell, E.; Rikken, G. L. J. A.; Avarvari, N. Electrical magnetochiral anisotropy in a bulk chiral molecular conductor. *Nat. Commun.* **2014**, *5*, 3757. (i) Train, C.; Gruselle, M.; Verdaguer, M. The fruitful introduction of chirality and control of absolute configurations in molecular magnets. *Chem. Soc. Rev.* **2011**, *40*, 3297-3312.

(6) (a) Casper, L. A.; Wursthorn, L.; Geppert, M.; Roser, P.; Linseis, M.; Drescher, M.; Winter, R. F. 4-Ferrocenylphenyl-Substituted Tritylium Dyes with Open and Interlinked C+Ar2 Entities: Redox Behavior, Electrochromism, and a Quantitative Study of the Dimerization of Their Neutral Radicals. *Organometallics* **2020**, *39*, 3275-3289. (b) Duxbury, D. F. The photochemistry and photophysics of triphenylmethane dyes in solid and liquid media. *Chem. Rev.* **1993**, *93*, 381-433.

(7) (a) Zhu, Z.; Zhang, D.; Xiao, T.; Fang, Y.-H.; Xiao, X.; Wang, X.-G.; Jiang, S.-D.; Zhao, D. Rational Design of an Air-Stable, High-Spin Diradical with Diazapyrene. *Angew. Chem. Int. Ed.* **2023**, *62*, e202314900. (b) Li, L.; Prindle, C. R.; Shi, W.; Nuckolls, C.; Venkataraman, L. Radical Single-Molecule Junctions. *J. Am. Chem. Soc.* **2023**, *145*, 18182-18204. (c) Heuer, A. M.; Coste, S. C.; Singh, G.; Mercado, B. Q.; Mayer, J. M. A Guide to Tris(4-Substituted)-triphenylmethyl Radicals. *J. Org. Chem.* **2023**, *88*, 9893-9901. (d) Poncelet, M.; Huffman, J. L.; Khramtsov, V. V.; Dhimitruka, I.; Driesschaert, B. Synthesis of hydroxyethyl tetrathiatriarylmethyl radicals OX063 and OX071. *RSC Adv.* **2019**, *9*, 35073-35076. (e) Kato, K.; Osuka, A. Platforms for Stable Carbon-Centered Radicals. *Angew. Chem. Int. Ed.* **2019**, *58*, 8978-8986. (f) Rösel, S.; Becker, J.; Allen, W. D.; Schreiner, P. R. Probing the Delicate Balance between Pauli Repulsion and London Dispersion with Triphenylmethyl Derivatives. *J. Am. Chem. Soc.* **2018**, *140*, 14421-14432. (g) Gomberg, M. Organic Radicals. *Chem. Rev.* **1924**, *1*, 91-141.

(8) (a) Murto, P.; Chowdhury, R.; Gorgon, S.; Guo, E.; Zeng, W.; Li, B.; Sun, Y.; Francis, H.; Friend, R. H.; Bronstein, H. Mesitylated trityl radicals, a platform for doublet emission: symmetry breaking, charge-transfer states and conjugated polymers. *Nat. Commun.* **2023**, *14*, 4147. (b) Abdurahman, A.; Wang, J.; Zhao, Y.; Li, P.; Shen, L.; Peng, Q. A Highly Stable Organic Luminescent Diradical. *Angew. Chem. Int. Ed.* **2023**, *62*, e202300772. (c) Li, Z.; Wang, J.; Liu, X.; Gao, P.; Li, G.; He, G.; Rao, B. Air-Stable Organoradical Boron Reagents. *Angew. Chem. Int. Ed.* **2023**, *62*, e2023o2835. (d) Murto, P.; Bronstein, H. Electro-optical π-radicals: design advances, applications and future perspectives. *J. Mater. Chem. C* **2022**, *10*, 7368-7403. (e) Chen, L.; Arnold, M.; Kittel, Y.; Blinder, R.; Jelezko, F.; Kuehne, A. J. C. 2,7-Substituted N-Carbazole Donors on Tris(2,4,6-trichlorophenyl)methyl Radicals with High Quantum Yield. *Adv. Opt. Mater.* **2022**, *10*, 2102101. (f) Liu, C.-H.; Hamzehpoor, E.; Sakai-Otsuka, Y.; Jadhav, T.; Perepichka, D. F. A Pure-Red Doublet Emission with 90 % Quantum Yield: Stable, Colorless, Iodinated Triphenylmethane Solid. *Angew. Chem. Int. Ed.* **2020**, *59*, 23030-23034. (g) Ratera, I.; Vidal-Gancedo, J.; Maspoch, D.; Bromley, S. T.; Crivillers, N.; Mas-Torrent, M. Perspectives for polychlorinated trityl radicals. *J. Mater. Chem. C* **2021**, *9*, 10610-10623. (h) Guo, H.; Peng, Q.; Chen, X.-K.; Gu, Q.; Dong, S.; Evans, E. W.; Gillett, A. J.; Ai, X.; Zhang, M.; Credgington, D.; Coropceanu, V.; Friend, R. H.; Brédas, J.-L.; Li, F. High stability and luminescence efficiency in donor–acceptor neutral radicals not following the Aufbau principle. *Nat. Mater.* **2019**, *18*, 977-984.

(9) (a) Li, Y.; Zhai, W.; Liao, Y.; Nie, J.; Han, G.; Song, Y.; Li, S.; Hou, J.; Liu, Y. Synthesis of Central Chirality-Containing Triarylmethanols and Triarylmethyl Radicals with Extraordinarily Stable Configurations. *J. Org. Chem.* **2019**, *84*, 11774-11782. (b) Ściebura, J.; Skowronek, P.; Gawronski, J. Trityl Ethers: Molecular Bevel Gears Reporting Chirality through Circular Dichroism Spectra. *Angew. Chem. Int. Ed.* **2009**, *48*, 7069-7072. (c) Mislow, K. Stereochemical consequences of correlated rotation in molecular propellers. *Acc. Chem. Res.* **1976**, *9*, 26-33.

(10) (a) Driesschaert, B.; Robiette, R.; Le Duff, C. S.; Collard, L.; Robeyns, K.; Gallez, B.; Marchand-Brynaert, J. Configurationally Stable Tris(tetrathioaryl)methyl Molecular Propellers. *Eur. J. Org. Chem.* **2012**, *2012*, 6517-6525. (b) Veciana, J.; Crespo, M. I. Dynamic HPLC: A Method for Determining Rate Constants, Energy Barriers, and Equilibrium Constants of Molecular Dynamic Processes. *Angew. Chem. Int. Ed.* **1991**, *30*, 74-76.

(11) (a) Mayorga Burrezo, P.; Jiménez, V. G.; Blasi, D.; Ratera, I.; Campaña, A. G.; Veciana, J. Organic Free Radicals as Circularly Polarized Luminescence Emitters. *Angew. Chem. Int. Ed.* **2019**, *58*, 16282-16288. (b) Mayorga-Burrezo, P.; Jiménez, V. G.; Blasi, D.; Parella, T.; Ratera, I.; Campaña, A. G.; Veciana, J. An Enantiopure Propeller-Like Trityl-Brominated Radical: Bringing Together a High Racemization Barrier and an Efficient Circularly Polarized Luminescent Magnetic Emitter. *Chem. Eur. J.* **2020**, *26*, 3776-3781.

(12) (a) Duan, J.; Shi, Y.; Zhao, F.; Li, C.; Duan, Z.; Zhang, N.; Chen, P. Chiral Luminescent Aza[7]helicenes Functionalized with a Triarylborane Acceptor and Near-Infrared-Emissive Doublet-State Radicals. *Inorg. Chem.* **2023**, 62, 15829–15833. (b) Stasiak, B.; Czapik, A.; Kwit, M. Dynamic Induction of Optical Activity in Triarylmethanols and Their Carbocations. *J. Org. Chem.* **2021**, *86*, 643-656. (c) Chen, C.-T.; Chao, S.-D.; Yen, K.-C.; Chen, C.-H.; Chou, I.-C.; Hon, S.-W. Chiral Triarylcarbenium Ions in Asymmetric Mukaiyama Aldol Additions. *J. Am. Chem. Soc.* **1997**, *119*, 11341-11342.

(13) (a) Gross, B. M.; Oestreich, M. The Trityl Cation Embedded into a [7]Helicene-Like Backbone: Preparation and Application as a Lewis Acid Catalyst. *Synthesis* **2021**, 53, 2512-2516. (b) Bosson, J.; Bisballe, N.; Laursen, B. W.; Lacour, J. Cationic Triarylcarbenium Helicenes: Synthesis, Resolution, and Applications. In *Helicenes: Synthesis, Properties and Applications*, Crassous, J., G. Stará, I., Starý, I. Eds.; Wiley, 2022; pp 127-165.

(14) Ueda, A.; Wasa, H.; Suzuki, S.; Okada, K.; Sato, K.; Takui, T.; Morita, Y. Chiral Stable Phenalenyl Radical: Synthesis, Electronic-Spin Structure, and Optical Properties of [4]Helicene-Structured Diazaphenalenyl. *Angew. Chem. Int. Ed.* **2012**, *51*, 6691-6695.

(15) (a) Shaikh, A. C.; Moutet, J.; Veleta, J. M.; Hossain, M. M.; Bloch, J.; Astashkin, A. V.; Gianetti, T. L. Persistent, highly localized, and tunable [4]helicene radicals. *Chem. Sci.* **2020**, *11*, 11060-11067. (b) Sørensen, T. J.; Nielsen, M. F.; Laursen, B. W. Synthesis and Stability of N,N′-Dialkyl-1,13-dimethoxyquinacridinium (DMQA+): A [4]Helicene with Multiple Redox States. *ChemPlusChem* **2014**, *79*, 1030-1035.

(16) (a) Crassous, J.; Stará, I. G.; Stary, I. *Helicenes: Synthesis, Properties, and Applications*; John Wiley & Sons, 2022. (b) Liu, W.; Qin, T.; Xie, W.; Yang, X. Catalytic Enantioselective Synthesis of Helicenes. *Chem. Eur. J.* **2022**, *28*, e202202369. (c) Stará, I. G.;

Starý, I. Helically Chiral Aromatics: The Synthesis of Helicenes by [2 + 2 + 2] Cycloisomerization of π-Electron Systems. *Acc. Chem. Res.* **2020**, *53*, 144-158. (d) Dhbaibi, K.; Favereau, L.; Crassous, J. Enantioenriched Helicenes and Helicenoids Containing Main-Group Elements (B, Si, N, P). *Chem. Rev.* **2019**, *119*, 8846-8953. (e) Chen, C.-F.; Shen, Y. *Helicene chemistry: from synthesis to applications*; Springer, 2016. (f) Gingras, M. One hundred years of helicene chemistry. Part 3: applications and properties of carbohelicenes. *Chem. Soc. Rev.* **2013**, *42*, 1051-1095.

(17) (a) Laleu, B.; Mobian, P.; Herse, C.; Laursen, B. W.; Hopfgartner, G.; Bernardinelli, G.; Lacour, J. Resolution of [4]Heterohelicenium Dyes with Unprecedented Pummerer-like Chemistry. *Angew. Chem. Int. Ed.* **2005**, *44*, 1879-1883. (b) Herse, C.; Bas, D.; Krebs, F. C.; Bürgi, T.; Weber, J.; Wesolowski, T.; Laursen, B. W.; Lacour, J. A Highly Configurationally Stable [4]Heterohelicenium Cation. *Angew. Chem. Int. Ed.* **2003**, *42*, 3162-3166.

(18) (a) Moutet, J.; Mills, D.; Hossain, M. M.; Gianetti, T. L. Increased performance of an all-organic redox flow battery model via nitration of the [4]helicenium DMQA ion electrolyte. *Mater. Adv.* **2022**, *3*, 216-223. (b) Nikolova, Y.; Fabri, B.; Moneva Lorente, P.; Guarnieri-Ibáñez, A.; de Aguirre, A.; Soda, Y.; Pescitelli, G.; Zinna, F.; Besnard, C.; Guénée, L.; Moreau, D.; Di Bari, L.; Bakker, E.; Poblador-Bahamonde, A. I.; Lacour, J. Chemo- and Regioselective Multiple C(sp^2)–H Insertions of Malonate Metal Carbenes for Late-Stage Functionalizations of Azahelicenes. *Angew. Chem. Int. Ed.* **2022**, *61*, e202210798. (c) Calogero, F.; Magagnano, G.; Potenti, S.; Pasca, F.; Fermi, A.; Gualandi, A.; Ceroni, P.; Bergamini, G.; Cozzi, P. G. Diastereoselective and enantioselective photoredox pinacol coupling promoted by titanium complexes with a red-absorbing organic dye. *Chem. Sci.* **2022**, *13*, 5973-5981. (d) Ondrisek, P.; Elie, M.; Pupier, M.; de Aguirre, A.; Poblador-Bahamonde, A. I.; Besnard, C.; Lacour, J. Acetylene Derivatives of Cationic Diazaoxatriangulenes and Diaza [4]Helicenes - Access to Red Emitters and Planar Chiral Stereochemical Traits. *Chem. Eur. J.* **2022**, *28*, e202104405. (e) Mei, L.; Veleta, J. M.; Gianetti, T. L. Helical Carbenium Ion: A Versatile Organic Photoredox Catalyst for Red-Light-Mediated Reactions. *J. Am. Chem. Soc.* **2020**, *142*, 12056-12061. (f) Duwald, R.; Bosson, J.; Pascal, S.; Grass, S.; Zinna, F.; Besnard, C.; Di Bari, L.; Jacquemin, D.; Lacour, J. Merging polyacenes and cationic helicenes: from weak to intense chiroptical properties in the far red region. *Chem. Sci.* **2020**, *11*, 1165-1169. (g) Hargenrader, G. N.; Weerasooriya, R. B.; Ilic, S.; Niklas, J.; Poluektov, O. G.; Glusac, K. D. Photoregeneration of Biomimetic Nicotinamide Adenine Dinucleotide Analogues via a Dye-Sensitized Approach. *ACS Appl. Energy Mater.* **2019**, *2*, 80-91. (h) Babič, A.; Pascal, S.; Duwald, R.; Moreau, D.; Lacour, J.; Allémann, E. [4]Helicene-squalene fluorescent nanoassemblies for specific targeting of mitochondria in live-cell imaging. *Adv. Funct. Mater.* **2017**, *27*, 1701839.

(19) (a) Guillemard, L.; Kaplaneris, N.; Ackermann, L.; Johansson, M. J. Late-stage C–H functionalization offers new opportunities in drug discovery. *Nat. Rev. Chem.* **2021**, 522–545. (b) Börgel, J.; Ritter, T. Late-Stage Functionalization. *Chem* **2020**, *6*, 1877-1887. (c) Jakubec, M.; Storch, J. Recent Advances in Functionalizations of Helicene Backbone. *J. Org. Chem.* **2020**, *85*, 13415-13428.

(20) On core compound **1**, electrophilic substitutions occur at position 6, but also 2 and 12 under strongly-acidic conditions, thanks to the electon-donating intracyclic nitrogen atoms. See ref 31 and Duwald, R.; Pascal, S.; Bosson, J.; Grass, S.; Besnard, C.; Bürgi, T.; Lacour, J. Enantiospecific Elongation of Cationic Helicenes by Electrophilic Functionalization at Terminal Ends. *Chem. Eur. J.* **2017**, *23*, 13596-13601.

(21) (a) Westerlund, F.; Hildebrandt, C. B.; Sørensen, T. J.; Laursen, B. W. Trihydroxytrioxatriangulene—An Extended Fluorescein and a Ratiometric pH Sensor. *Chem. Eur. J.* **2010**, *16*, 2992-2996. (b) Sørensen, T. J.; Laursen, B. W. Synthesis and Optical Properties of Trioxatriangulenium Dyes with One and Two Peripheral Amino Substituents. *J. Org. Chem.* **2010**, *75*, 6182-6190.

(22) Noguchi, H.; Hirose, T.; Yokoyama, S.; Matsuda, K. Fluorescence behavior of 2,6,10-trisubstituted 4,8,12-triazatriangulene cations in solution and in the solid state. *CrystEngComm* **2016**, *18*, 7377-7383.

(23) (a) Yu, I. F.; Wilson, J. W.; Hartwig, J. F. Transition-Metal-Catalyzed Silylation and Borylation of C–H Bonds for the Synthesis and Functionalization of Complex Molecules. *Chem. Rev.* **2023**, *123*, 11619-11663. (b) Mihai, M. T.; Genov, G. R.; Phipps, R. J. Access to the meta position of arenes through transition metal catalysed C–H bond functionalisation: a focus on metals other than palladium. *Chem. Soc. Rev.* **2018**, *47*, 149-171. (c) Preshlock, S. M.; Ghaffari, B.; Maligres, P. E.; Krska, S. W.; Maleczka, R. E.; Smith, M. R. High-Throughput Optimization of Ir-Catalyzed C–H Borylation: A Tutorial for Practical Applications. *J. Am. Chem. Soc.* **2013**, *135*, 7572-7582. (d) Ishiyama, T.; Takagi, J.; Ishida, K.; Miyaura, N.; Anastasi, N. R.; Hartwig, J. F. Mild Iridium-Catalyzed Borylation of Arenes. High Turnover Numbers, Room Temperature Reactions, and Isolation of a Potential Intermediate. *J. Am. Chem. Soc.* **2002**, *124*, 390-391.

(24) Frédéric, L.; Fabri, B.; Guénée, L.; Zinna, F.; Di Bari, L.; Lacour, J. Triple Regioselective Functionalization of Cationic [4]Helicenes via Iridium-Catalyzed Borylation and Suzuki Cross-Coupling Reactivity. *Chem. Eur. J.* **2022**, *28*, e2022201853.

(25) (a) Ishii, H.; Minegishi, K.; Nagatsu, K.; Zhang, M.-R. Pd(0)-mediated [^{11}C]carbonylation of aryl and heteroaryl boronic acid pinacol esters with [^{11}C]carbon monoxide under ambient conditions and a facile process for the conversion of [carbonyl-^{11}C]esters to [carbonyl-^{11}C]amides. *Tetrahedron* **2015**, *71*, 1588-1596. (b) Yamamoto, Y. The First General and Selective Palladium(II)-Catalyzed Alkoxycarbonylation of Arylboronates: Interplay among Benzoquinone-Ligated Palladium(0) Complex, Organoboron, and Alcohol Solvent. *Adv. Synth. Catal.* **2010**, *352*, 478-492.

(26) Under one-pot conditions, the excess of PBQ is most probably necessary to counterbalance the preceding reductive Ir-catalyzed conditions. See ref 24.

(27) Strickler, S. J.; Berg, R. A. Relationship between Absorption Intensity and Fluorescence Lifetime of Molecules. *The Journal of Chemical Physics* **1962**, *37*, 814-822.

(28) For a theoretical prediction of ECD properties, see Elm, J.; Lykkebo, J.; Sørensen, T. J.; Laursen, B. W.; Mikkelsen, K. V. Obtaining Enhanced Circular Dichroism in [4]Heterohelicenium Analogues. *J. Phys. Chem. A* **2012**, *116*, 8744-8752.

(29) (a) Cei, M.; Di Bari, L.; Zinna, F. Circularly polarized luminescence of helicenes: A data-informed insight. *Chirality* **2023**, *35*, 192-210. (b) Mori, T. Chiroptical Properties of Symmetric Double, Triple, and Multiple Helicenes. *Chem. Rev.* **2021**, *121*, 2373-2412. (c) Tanaka, H.; Inoue, Y.; Mori, T. Circularly Polarized Luminescence and Circular Dichroisms in Small Organic Molecules: Correlation between Excitation and Emission Dissymmetry Factors. *ChemPhotoChem* **2018**, *2*, 386-402.

(30) Arrico, L.; Di Bari, L.; Zinna, F. Quantifying the Overall Efficiency of Circularly Polarized Emitters. *Chem. Eur. J.* **2021**, *27*, 2920-2934.

(31) Delgado, I. H.; Pascal, S.; Wallabregue, A.; Duwald, R.; Besnard, C.; Guénée, L.; Nançoz, C.; Vauthey, E.; Tovar, R. C.; Lunkley, J. L.; Muller, G.; Lacour, J. Functionalized cationic [4]helicenes with unique tuning of absorption, fluorescence and chiroptical properties up to the far-red range. *Chem. Sci.* **2016**, *7*, 4685-4693.

(32) Computed MOs for selected *meta* derivatives (OMe and CO_2Me) are shown in Figures S79-S80 for comparison.

(33) (a) Dewar, M. J. S.; Dougherty, R. C. *The PMO theory of organic chemistry*; Plenum Press New York, 1975. (b) Rosenberg, M.; Rostgaard, K. R.; Liao, Z.; Madsen, A. Ø.; Martinez, K. L.; Vosch, T.; Laursen, B. W. Design, synthesis, and time-gated cell imaging of carbon-bridged triangulenium dyes with long fluorescence lifetime and red emission. *Chem. Sci.* **2018**, *9*, 3122-3130.

(34) McDaniel, D. H.; Brown, H. C. An Extended Table of Hammett Substitutent Constants Based on the Ionization of Substituted Benzoic Acids. *J. Org. Chem.* **1958**, *23*, 420-427.

(35) (a) Armet, O.; Veciana, J.; Rovira, C.; Riera, J.; Castaner, J.; Molins, E.; Rius, J.; Miravitlles, C.; Olivella, S.; Brichfeus, J. Inert carbon free radicals. 8. Polychlorotriphenylmethyl radicals: synthesis, structure, and spin-density distribution. *J. Phys. Chem.* **1987**, *91*, 5608-5616. (b) Ballester, M.; Riera-Figueras, J.; Castaner, J.; Badfa, C.; Monso, J. M. Inert carbon free radicals. I. Perchlorodiphenylmethyl and perchlorotriphenylmethyl radical series. *J. Am. Chem. Soc.* **1971**, *93*, 2215-2225.

(36) (a) Abdurahman, A.; Hele, T. J. H.; Gu, Q.; Zhang, J.; Peng, Q.; Zhang, M.; Friend, R. H.; Li, F.; Evans, E. W. Understanding the luminescent nature of organic radicals for efficient doublet emitters and pure-red light-emitting diodes. *Nat. Mater.* **2020**, *19*, 1224-1229. (b) Dong, S.; Xu, W.; Guo, H.; Yan, W.; Zhang, M.; Li, F. Effects of substituents on luminescent efficiency of stable triaryl methyl radicals. *Phys. Chem. Chem. Phys.* **2018**, *20*, 18657-18662. (c) Gamero, V.; Velasco, D.; Latorre, S.; López-Calahorra, F.; Brillas, E.; Juliá, L. [4-(N-Carbazolyl)-2,6-dichlorophenyl]bis(2,4,6-trichlorophenyl)methyl radical an efficient red light-emitting paramagnetic molecule. *Tetrahedron Lett.* **2006**, *47*, 2305-2309.

(37) (a) Ueda, A.; Wasa, H.; Nishida, S.; Kanzaki, Y.; Sato, K.; Shiomi, D.; Takui, T.; Morita, Y. An Extremely Redox-Active Air-Stable Neutral π Radical: Dicyanomethylene-Substituted Triangulene with a Threefold Symmetry. *Chem. Eur. J.* **2012**, *18*, 16272-16276. (b) Neugebauer, F. A.; Hellwinkel, D.; Aulmich, G. E.S.R. study of 12,12c-dihydro-4,4,8,8,12,12-hexamethyl-4H, 8H-dibenzo [cd,mn] pyren-12c-yl, a planar triphenylmethyl. *Tetrahedron Lett.* **1978**, *19*, 4871-4874. (c) Sabacky, M. J.; Johnson, C. S.; Smith, R. G.; Gutowsky, H. S.; Martin, J. C. Triarylmethyl Radicals. Synthesis and Electron Spin Resonance Studies of Sesquixanthydryl Dimer and Related Compounds. *J. Am. Chem. Soc.* **1967**, *89*, 2054-2058.

(38) Krejčik, M.; Daněk, M.; Hartl, F. Simple construction of an infrared optically transparent thin-layer electrochemical cell: Applications to the redox reactions of ferrocene, $Mn_2(CO)_{10}$ and $Mn(CO)_3$(3,5-di-t-butyl-catecholate). *J. Electroanal. Chem. Interfacial Electrochem.* **1991**, *317*, 179-187.

(39) Compound **3** showed very little stability upon bulk electrolysis; the ECD spectra obtained for enantiopure solutions are reported in the SI (Figure S37).

(40) During measurements, evidence for a (partial) racemization of the radical species could not be found. Compounds **4**$^{\bullet}$ and **5**$^{\bullet}$ present, most probably, a configurational stability similar to **II**. See ref 14.

(41) This good agreement is also observed in the cationic series (Figures S65 and S67); ECD data confirming hence the absolute configuration assignment inferred from the enantiospecific synthesis.

(42) (a) Kasemthaveechok, S.; Abella, L.; Jean, M.; Cordier, M.; Vanthuyne, N.; Guizouarn, T.; Cador, O.; Autschbach, J.; Crassous, J.; Favereau, L. Carbazole Isomerism in Helical Radical Cations: Spin Delocalization and SOMO–HOMO Level Inversion in the Diradical State. *J. Am. Chem. Soc.* **2022**, *144*, 7253-7263. (b) Abella, L.; Crassous, J.; Favereau, L.; Autschbach, J. Why is the Energy of the Singly Occupied Orbital in Some Radicals below the Highest Occupied Orbital Energy? *Chem. Mater.* **2021**, *33*, 3678-3691. (c) Rajca, A.; Shu, C.; Zhang, H.; Zhang, S.; Wang, H.; Rajca, S. Thiophene-Based Double Helices: Radical Cations with SOMO–HOMO Energy Level Inversion. *Photochem. Photobiol.* **2021**, *97*, 1376-1390.

(43) Connelly, N. G.; Geiger, W. E. Chemical Redox Agents for Organometallic Chemistry. *Chem. Rev.* **1996**, *96*, 877-910.

(44) It can be hypothesized that **4**$^{\bullet}$, being slightly less stable than **5**$^{\bullet}$, is more sensitive to the presence of impurities in the chemical reductant.

(45) Stoll, S.; Schweiger, A. EasySpin, a comprehensive software package for spectral simulation and analysis in EPR. *J. Magn. Reson.* **2006**, *178*, 42-55.

(46) Previously, examples on similar structures in inert trifluoro toluene presented lifetimes up to 3.5 h. See ref 15a.

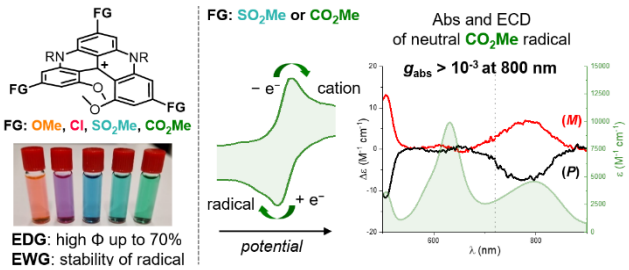
FG
RN
NR
FG
FG
FG: OMe, Cl, SO2Me, CO2Me
EDG: high Φ up to 70%
EWG: stability of radical
FG: SO2Me or CO2Me
− e⁻
cation
radical
+ e⁻
potential
Abs and ECD
of neutral CO2Me radical
gabs > 10-3 at 800 nm
(M)
(P)
Δε (M-1 cm-1)
ε (M-1 cm-1)
λ (nm)